Intelligent Perception of Coseismic Landslide Migration Areas Along Sichuan–Tibet Railway

Wenyang Shi ⬤ and Ping Lu

Abstract—The geological conditions along Sichuan–Railway are complex, and frequently-occurred landslides have brought severe challenges to the railway construction. Therefore, a complete and accurate landslide perception can provide references for railway route selection and landslide risk governance. In this study, we utilized change vector analysis, principal component analysis, and independent component analysis (ICA) for change detection images generation, and then adopted the multithreshold method to produce the training sample templates for landslides and nonlandslides, respectively. The Markov random field (MRF) algorithm was further used to extract the optimal landslide objects. In particular, we tested the performance of the proposed approach using the Sentinel-2 datasets in a rapid perception of the coseismic landslides for the Nyingchi event that occurred on 18 November 2017 and affected the railway construction. We further calculated completeness, correctness, accuracy, F1-score, and Kappa coefficient, for a quantitative evaluation of landslide perception results. We found that the ICA-based change detection in MRF can extract landslides more completely and accurately. This study set up with the aim to assess the effectiveness and applicability of the proposed method in mapping landslide migration areas under complex geological conditions along the Sichuan–Tibet Railway, which offers a comprehensively intelligent approach to supporting the hazard mitigation for a safe railway construction and operation.

Index Terms—Change detection, landslide, Markov random field (MRF), Nyingchi event, Sentinel-2, Sichuan–Tibet Railway.

I. INTRODUCTION

S ICHUAN–TIBET Railway, which connects Chengdu (Sichuan Province) and Lhasa (Tibet Province), is an epic project that is currently under construction in China. The difficulty of constructing Sichuan–Tibet Railway is due to the steep terrain, complex geological settings, active tectonics, and the numerous triggered natural hazards that exist in the Southeastern Tibetan Plateau [1], [2]. In particular, the railway is often affected by the squeezed and uplifted plates, fragile geological conditions and rock fragmentation, and river erosion [3]. Landslides are typical natural hazards that occurred along the railway, resulting in frequent river blockage and flooding, which can directly affect the planning and construction of the railway [1], [4], [5]. Thus, a complete and accurate mapping of landslide migration areas is the key point in the hazard assessment and mitigation of landslide disasters during the railway construction and operation [6], which may need an intelligent perception of landslide hazards.

Prior studies focused on landslide perception mainly through visual interpretation from remote sensing images [7]–[9]. The visual interpretation method is actually very accurate, but not so effective after major events because it is time-consuming. Thus, the visual interpretation method cannot accurately analyze landslide disasters in time to provide reference for engineering construction. In recent decades, there are two basic approaches usually adopted in practice for landslide mapping [9], [10], namely pixel-based and object-oriented method. The pixel-based method is effective in extracting information from low- and medium-resolution remote sensing images. However, for high-resolution remote sensing images, the pixel-based method may have difficulty in effectively extracting the landslide information from images due to the salt and pepper noises, thus resulting in poor classification accuracy [11], [12]. The object-oriented method uses the spectral, spatial, and morphometric information of pixel groups as basic units for information extraction, thereby improving the performance of image classification. For example, Lu *et al.* [13] introduced an object-oriented approach using the very high-resolution optical images for landslide rapid mapping. Martha *et al.* [14] and [15] proposed a semiautomatic approach based on the object-oriented change detection method to detect land cover changes, which can perform fully automatic multiscale optimization for specific problems in image segmentation, and present multispectral analysis at object level. Chen *et al.* [16] integrated random forest and mathematical morphology into object-oriented analysis (OOA) for landslide mapping from ZY-3 imageries. It is argued that landslide mapping through the object-oriented method may achieve better accuracy than pixel-based approach [11]. Despite that OOA may achieve better landslide mapping accuracy, its usefulness highly depends on a high-quality image segmentation, in which over- and under-segmentation need to be maximally reduced.

Mondini *et al.* [17] adopted three change detection methods: normalized difference vegetation index (NDVI), principal component analysis (PCA), and independent component analysis (ICA) for change detection images (CDIs) generation, and then used three classification models to identify landslides and nonlandslides. Although this method can achieve landslide mapping well, they may neglect the spatial relationship between the landslides and its surroundings environment. Lv *et al.* [18] developed a land cover change detection approach based on

adaptive contextual information, and calculated the change range of the center pixel based on the distance between adaptive extension regions to obtain land cover change information. Kurtz *et al.* [19] proposed a top-down multiresolution hierarchical approach that can protect landslide mapping results from the large size and different levels of details in multiresolution satellite images, although a number of parameters need to be determined and may accordingly reduce the accuracy for landslide mapping. Yi *et al.* [20] developed a deep-learning-based approach for coseismic landslide detection from RapidEye imagery. Ye *et al.* [21] fulfilled landslide detection from hyperspectral data using deep learning constrains. Cai *et al.* [22] established a landslide sample library by adding environmental factors using densely connected convolutional networks. Duric *et al*. [23] used PCA and semiautomatic classification methods to map landslide inventory in very high and high (VHR-HR) resolution images (i.e., Pléiades, WorldView-2, and SPOT-6 satellite images). VHR-HR images have advantages in image classification due to their high spatial resolution, although there is no evidence showing that this method is applicable to low- and medium-resolution images. To further improve the performance of landslide mapping, Lu *et al.* [24] developed change detection-based NDVI, change vector analysis (CVA), PCA, and ICA methods for CDIs generation from the multisensor data. They verified the performance of different change detection methods used in Markov random field (MRF) and applied them to map landslides triggered by rainfall, earthquakes, and typhoons. The landslide mapping results and accuracy evaluation showed that their proposed method has a wide range of applications and a high degree of automation. However, the usefulness of change detection-based MRF has not been fully exploited in complex geological conditions where huge elevation differences, active tectonics, and complicated triggering mechanism of landslides are prevalent.

To fill the gap of lacking application under complex geological conditions, we developed change detection-based MRF for intelligent perception of landslide migration areas along Sichuan–Tibet Railway. In particular, we focused on the 2017 Nyingchi landslide event along the railway based on the bitemporal Sentinel-2 optical images. We adopted three change detection techniques (CVA, PCA, and ICA) with multithresholds in MRF to justify the improvements of image transformation over spectral subtraction, so as to obtain a more reliable map of landslide migration areas. We anticipated the proposed approach for landslide migration area mapping can provide fundamental references for disaster risk management on the railway construction and operation.

II. Event and Data

On 18 November 2017, a magnitude 6.9 earthquake struck Nyingchi (Tibet). The epicenter was located at 29.75° N and 96.02° E, and the focal depth was 10 km [25]. Because the epicenter was located in a sparsely populated area, there was less direct loss of human lives and properties. However, the Nyingchi earthquake triggered more than 1820 landslides, affecting an area of approximately 527 km^2 [26], which had a huge impact on the mountains around Yarlung Zangbo River,
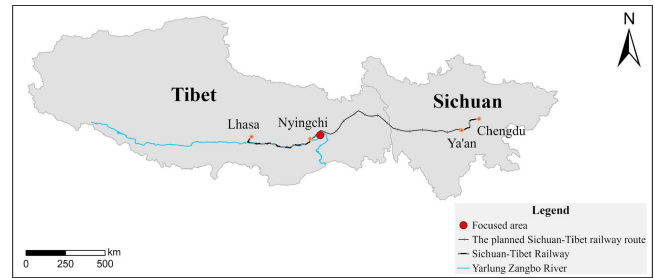

Fig. 1. Route of Sichuan–Tibet Railway.

and the river gradually brought a large amount of sedimentation mud downstream [27]. Thus, the Nyingchi event has left great potential threats to the subsequent construction of Sichuan–Tibet Railway. In addition, the study area is located in the Yarlung Zangbo River Grand Canyon region of the eastern Himalayas of Tibet, which is featured as the deepest valley of the world with the elevation ranging from 442 to 7782 m, and the average slopes on both sides are above 45° [28]. Due to the temperature and humidity of Indian Ocean flow north along the canyon, abundant precipitation during the rainy season can be formed, thus further increasing the risks of mountain hazards such as shallow landslides and debris flows. Fig. 1 shows the route of Sichuan–Tibet Railway and the focused area for intelligent perception of landslide migration areas in this study.

We used the Sentinel-2 optical data for landslide perception after the 2017 Nyingchi event. The Sentinel-2 satellite is equipped with a multispectral imager (MSI) with a height of 786 km, which can cover 13 spectral bands with an orbit width of 290 km [29]. Among them, Sentinel-2 can provide four 10 m bands (blue, green, red, and NIR), six 20 m bands and three 60 m bands. The revisit period of one satellite is ten days, and the revisit period of two satellites is five days [30], [31]. The red and NIR bands were found adequately represent the land cover changes brought by coseismic landslides [24] and accordingly these two bands were used in this study to reduce data redundancy. The Sentinel-2 Level-2A product used in this study case was obtained by preprocessing the Level-1C data through Sen2cor [32], [33]. The pre [see Fig. 2(a)] and postevent [see Fig. 2(b)] Sentinel-2 Level-1C multispectral images were collected on 9 May 2017 and 8 June 2018, respectively. These two images are the closest Sentienl-2 datasets before and after the earthquake event that are unaffected by clouds. These Sentinel-2 data were downloaded from the European Space Agency Sentinel-2 Preoperations Hub[1] for free.

III. Methodology

The proposed method used to map Nyingchi event can be divided into the following three steps. The first step is to generate CDIs by using three change detection algorithms (i.e., CVA, PCA, and ICA). The second step is to produce training samples for landslides and nonlandslides by using the multithreshold method. The last step in this process is to adopt MRF to eliminate
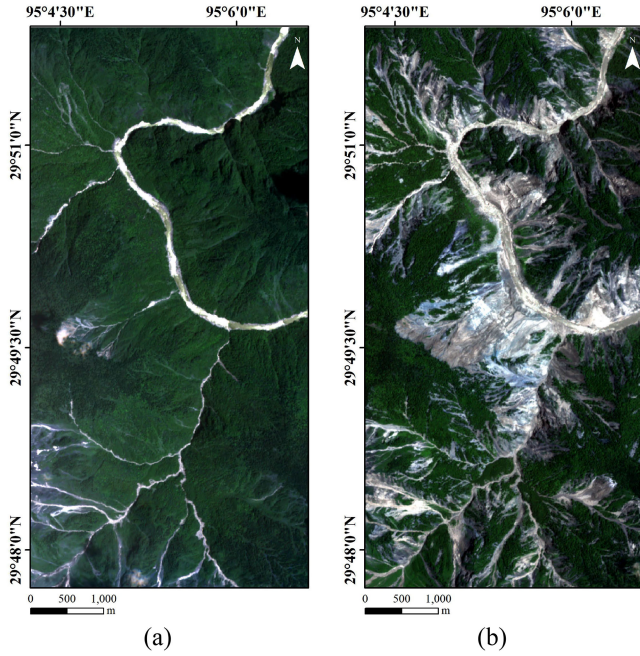
---

[1][Online]. Available: https://scihub.copernicus.eu/

Fig. 2. 10 m Sentinel-2 true color images for landslide perception in Nyingchi: (a) pre and (b) postevent images.

Fig. 3. Flowchart of the proposed methodology.

misclassification errors to obtain reliable landslide mapping results. The flowchart of the proposed methodology is shown in Fig. 3.

A. Change Detection Approaches

1) Change Vector Analysis: We used the CVA approach on multiple bands between the bitemporal images to identify image differences, and to obtain the change values of the corresponding pixels in each band [34]. The difference map can fully display the land cover change information on changed areas, thereby identifying landslide and nonlandslide objects. CVA can be defined as follows [35]:

$$\rho(I) = \left[\sum_{b=1}^{n}\left(I_{t1} - I_{t2}\right)\right]^{1/2} \quad (1)$$

where $\rho(I)$ represents the value of the pixel I, I_{t1}, and I_{t2} represent the value of the pixel I at t_1 and t_2, respectively. b is the band number. If the pixel value $\rho(I)$ in CDI is large, it will be considered as a landslide candidate. Thus, CVA can intuitively reflect the difference in the pixel value of each band in the pre and postevent images, and accordingly show land cover changes brought by landslides.

2) Principal Component Analysis: PCA regards multiple bands in the multispectral image as a multidimensional dataset, and obtains multiple principal components by performing PCA transformation on them [35]. The first few principal components after PCA contain the main feature information, and the noises that are relatively small remain on the minor components [36]. Those extracted principal components are considered to highlight the change information and suppress noises. PCA is defined
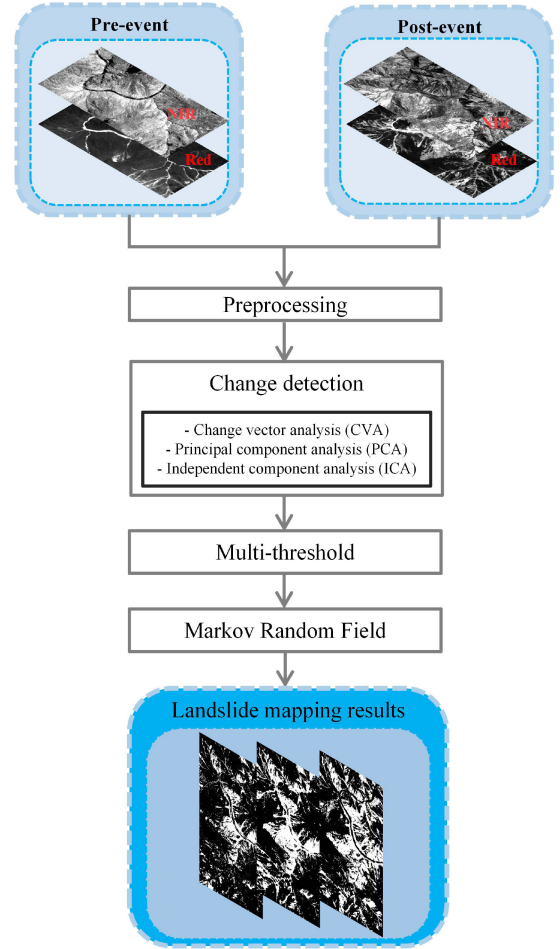
as follows [24]:

$$C = \mathrm{cov}(X, Y, Z, A)$$

$$= \begin{pmatrix} \mathrm{cov}(x,x)\,\mathrm{cov}(x,y)\,\mathrm{cov}(x,z) & \mathrm{cov}(x,a) \\ \mathrm{cov}(y,x)\,\mathrm{cov}(y,y)\,\mathrm{cov}(y,z) & \mathrm{cov}(y,a) \\ \mathrm{cov}(z,x)\,\mathrm{cov}(z,y)\,\mathrm{cov}(z,z) & \mathrm{cov}(z,a) \\ \mathrm{cov}(a,x)\,\mathrm{cov}(a,y)\,\mathrm{cov}(a,z) & \mathrm{cov}(a,a) \end{pmatrix} \quad (2)$$

where $cov\,(\cdot)$ represents covariance. X, Y, Z, and A are the red and NIR bands in the bitemporal images minus their means. In this study, the red and NIR bands were transformed into four component images through PCA. Through the initial visual inspection, we found that the second component is mostly related to landslides and therefore it was selected as the CDI.

3) Independent Component Analysis: The ICA-based change detection is to decompose a set of mixed signals into independent components to differentiate independent signals and suppress the Gaussian noises [27]. Therefore, ICA can separate the landslide relevant information in multispectral and multitemporal remote sensing images and convert them into independent parts, thereby enhancing the change information.
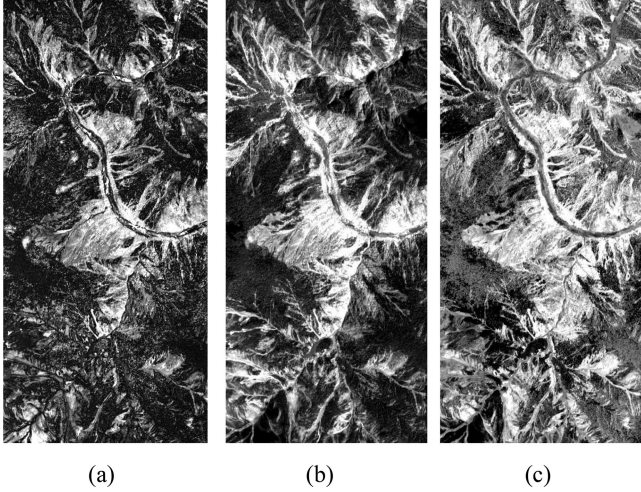
Fig. 4. CDIs generated by (a) CVA, (b) PCA, and (c) ICA.

Fig. 5. Training samples generated by: (a) CVA, (b) PCA, and (c) ICA-based change detection and multithreshold methods.

ICA is defined by [24]

$$\begin{pmatrix} x_1 \\ x_2 \\ x_3 \\ x_4 \end{pmatrix} = A \begin{pmatrix} s_1 \\ s_2 \\ s_3 \\ s_4 \end{pmatrix} \tag{3}$$

where x is the multitemporal spectral bands that are separated into statistically independent components s through the ICA transformation. A is the mixing matrix. Similar to PCA, the second component of ICA was chosen for the CDI generation because it appears to reflect the information brought by the occurrence of landslides.

Fig. 4(a)–(c) show the CDIs derived from CVA, PCA, and ICA, respectively. Brighter pixels represent landslides, whereas darker pixels indicate nonlandslide objects. In the next step, the multithreshold method was used for the further accurate landslide mapping.

B. Multithreshold Method

The multithreshold method is an effective approach for image segmentation [10]. It uses the differences between the targets and background in an image to classify pixels, and then sets the thresholds to achieve the separation between targets and the background. We used the multithreshold method to automatically obtain landslide training samples from the previously derived CDI images. The multithreshold algorithm is defined as (4) shown at bottom of this page, where I_{CDI} is the pixel value in CDI, μ_{CDI}, and σ_{CDI} are the mean and standard deviation of CDI, respectively. $T, \Delta T (T \in R)$ are constants, which are the thresholds for obtaining landslide and nonlandslide training samples, respectively. The optimal parameters of T and ΔT were set to 0.6 and 0.8, respectively, through trial and error in this
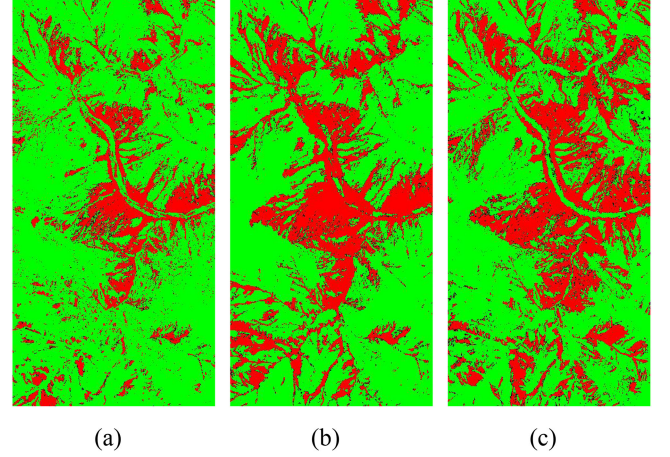
study. We experimented the values of T and ΔT to generate CDIs ranging from 0 to 2.0, with an interval value of 0.2 [24]. μ_{CDI} was calculated by accumulating the pixel values of the image and divided by the total number of pixels. σ_{CDI} can reflect the degree of dispersion of a dataset, which is calculated as follows:

$$\sigma_{CDI} = \sqrt{\frac{1}{N} \sum_{i=1}^{N} (I_i - \mu)^2} \tag{5}$$

where N is the total number of pixels. In CDIs, the greater value of a pixel, the more likely it belongs to a landslide object; otherwise, it is preferably classified as nonlandslides. Thus, if I_{CDI} in (4) is equal to or greater than $\mu_{CDI} + (T + \Delta T) * \sigma_{CDI}$, it can be regarded as a landslide training sample, which is represented by red pixels as shown in Fig. 5. If I_{CDI} is equal to or less than $\mu_{CDI} + T * \sigma_{CDI}$, it can be regarded as a nonlandslide training sample (green pixels in Fig. 5). To increase the reliability of landslide mapping, the MRF approach was further used to reclassify the uncertain areas into landslides or nonlandslides.

C. MRF for Accurate Landslide Mapping

Although the change detection and multithreshold methods for CDIs can offer decent performance, uncertain areas still exist, and accordingly we used the MRF approach to refine the landslide mapping accuracy. MRF is an image segmentation algorithm based on the statistical mechanisms. This method considers that pixels in an image are highly correlated with their neighbors, and meanwhile less affected by pixels outside the neighbors [24]. Therefore, MRF combines the contextual information around the pixels in the entire image, which can

$$I_{CDI} = \begin{cases} landslide & I_{CDI} \geq \mu_{CDI} + (T + \Delta T) * \sigma_{CDI} \\ uncertain\ area & \mu_{CDI} + (T + \Delta T) * \sigma_{CDI} > I_{CDI} > \mu_{CDI} + T * \sigma_{CDI} \\ non - landslide & I_{CDI} \leq \mu_{CDI} + T * \sigma_{CDI} \end{cases} \tag{4}$$
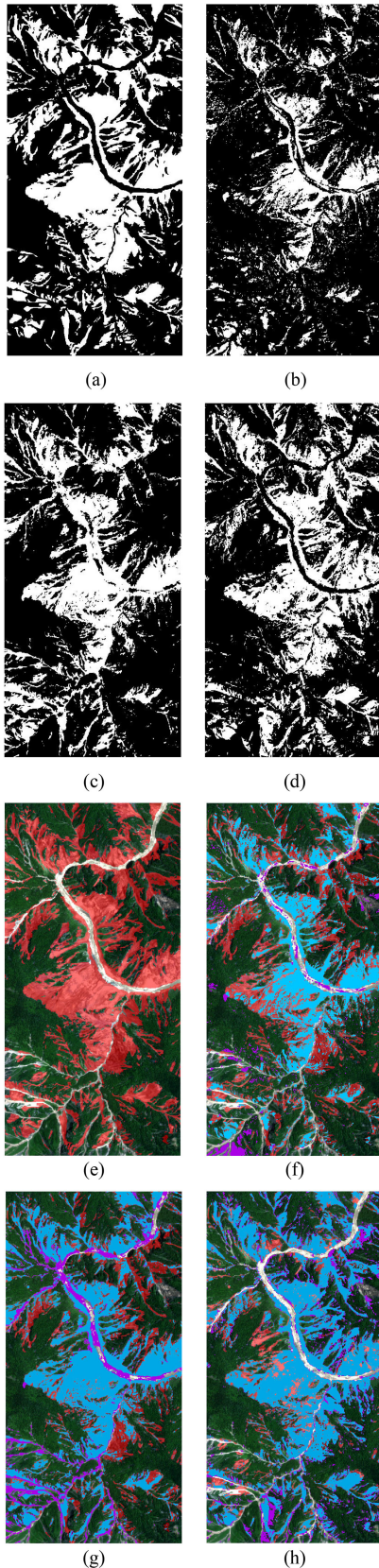
Fig. 6. (a) Binary maps of landslide ground truths. (b)–(d) Landslide mapping results generated by: (b) CVA, (c) PCA, and (d) ICA-based MRF. (e) Ground truths (red) overlaid on the post-event Sentinel-2 image. (f), (g), and (h) Mapped landslides (purple) in (b), (c), and (d) superimposed on ground truths (red), respectively, and their overlapped parts are shown in blue.

provide the prior local structure information for image classification to obtain better classification accuracy. For this purpose, we constructed an energy function to represent the correlations between adjacent pixels, which is defined as follows [27]:

$$E(L) = E_u(L) + \lambda * E_p(L) \tag{6}$$

$$\hat{L} = argmin E(L) \tag{7}$$

where $E_u(L)$ and $E_P(L)$ are the regional and boundary energy items, respectively. λ is the balance coefficient used to adjust the relative weight between these two items, which was set at a fixed value of 50 in this study. $L = (l_1, l_2, \ldots, l_n)$ is the minimum energy function corresponding to the label set, and it is also a measure of global quality evaluation. The value of l_i is 0 or 1, which corresponds to the background and the landslide target, respectively, and n is the total number of pixels in the image.

IV. RESULTS

The results of the binary images [see Fig. 6(a)] show the ground truth for the Nyingchi event, which was manually digitized through the visual interpretation of the landslide change information from the pre and postevent images. Fig. 6(b)–(d) show the landslide mapping results generated by CVA-, PCA-, and ICA-based MRF, respectively. Fig. 6(e) shows the ground truth map overlaid on the post-landslide Sentinel-2 truth color image (red pixels). Visual comparisons for the extraction results from each algorithm are displayed in Fig. 6(f)–(h). Among them, the mapped landslides (purple pixels) are superimposed on the ground truth map (red pixels), and the overlapped areas are displayed in blue pixels to represent the correctly detected landslides. Compared with the ground truths, it clearly demonstrates that the proposed method for landslide perception with ICA [see Fig. 6(h)] can produce less misclassified pixels (i.e., red and purple areas), which shows better performance than the results from PCA [see Fig. 6(f)] and CVA [see Fig. 6(g)].

To further investigate the effectiveness of CVA-, PCA-, and ICA-based MRF, the following five evaluation indices: *Completeness*, *Correctness*, *Accuracy*, *F1-score*, and *Kappa coefficient* were adopted to evaluate the landslide migration area perception performances [37]. In this article, the *Completeness*, *Correctness*, *Accuracy*, *F1-score*, and *Kappa coefficient* are defined as follows:

$$Completeness = \frac{A_0}{A_r} \tag{8}$$

$$Correctness = \frac{A_0}{A_e} \tag{9}$$

$$Accuracy = \frac{A_0 + A_n}{N} \tag{10}$$

$$F1 - score = \frac{2 * Completeness * Correctness}{Completeness + Correctness} \tag{11}$$

$$Kappa\ coefficient = \frac{Accuracy - p_e}{1 - p_e} \tag{12}$$

where A_0 is the total pixel number of the correctly mapped landslides, A_r is the pixel number of the landslide ground truth

TABLE I
QUANTITATIVE EVALUATION RESULTS ON LANDSLIDE PERCEPTION

Class			Ground truth						Total
			The pixel number of the landslides			The pixel number of the non-landslides			
			CVA	PCA-2	ICA-2	CVA	PCA-2	ICA-2	
Landslide mapping results	The pixel number of mapped landslides	CVA	49,835			8,245			58,080
		PCA-2		69,968			18,060		88,028
		ICA-2			82,377			16,823	99,200
	The pixel number of mapped non-landslides	CVA	55,299			184,226			239,525
		PCA-2		35,166			174,411		209,577
		ICA-2			22,757			175,648	198,405
Total			105,134	105,134	105,134	192,471	192,471	192,471	
Completeness			47.40%	66.55%	78.35%				
Correctness			85.80%	79.48%	83.04%				
Accuracy			78.65%	82.12%	86.70%				
F1-score			0.61	0.72	0.81				
Kappa coefficient			0.48	0.59	0.71				

map, A_e is the pixel number of the landslide mapping results, A_n is the pixel number of the correctly mapped nonlandslides, and N is the total pixel number of the landslides and nonlandslides. In (12), p_e is calculated as follows:

$$p_e = \frac{A_e \cdot A_r + (N - A_e) \cdot (N - A_r)}{N^2}. \qquad (13)$$

The above-mentioned quantitative evaluation results for landslide migration area perception from CVA-, PCA-, and ICA-based MRF are summarized in Table I.

Table I is a confusion matrix to show the landslide migration area mapping results generated from CVA-, PCA-, and ICA-based MRF. The completeness for the mapping results of ICA-2 outperforms CVA and PCA-2 by 30.95% and 11.80%, respectively. The correctness for the landslide mapping results of CVA, PCA-2, and ICA-2 are 85.80%, 79.48%, and 83.04%, respectively. The accuracy for the landslide mapping results increased from 78.65% (CVA) and 82.12% (PCA-2) to 86.70% (ICA-2). The F1-score and Kappa coefficient for ICA-2 are up to 0.81 and 0.71, whereas the results for CVA and PCA-2 are 0.61 and 0.48, 0.72, and 0.59, respectively. The quantitative comparisons in Table I confirms that the ICA-based MRF can render better performances on landslide migration area perception for the Nyingchi event that affected the construction of Sichuan–Tibet Railway.

V. DISCUSSION

In accordance with the landslide mapping results presented by Lu *et al.* [24], it turns out that the change detection-based MRF can obtain better accuracy and performance in landslide perception. However, the produced landslide migration area maps and some quantitative evaluations suggest that potential weakness may exist in the proposed method.

It can be seen that in Fig. 6 (a)–(c), the coseismic landslides are concentrated on both sides of the Yarlung Zangbo River [27]. The performance of the results mapped by CVA-based MRF [see Fig. 6(a)] shows lower accuracy. This is because CVA uses the bitemporal images in the same area to perform the difference to obtain the grayscale change of each pixel. However, the landslide in shadow areas may have similar spectral values to the surroundings, which can greatly increase the difficulty in

landslide detection. Therefore, Fig. 6(a) shows lower completeness landslide mapping results. Moreover, the result of PCA [see Fig. 6(b)] used in MRF produced more noises and thus may misclassify the Yarlung Zangbo River as landslides. Although the PCA algorithm is suitable for the transformation of all bands in a multispectral image, it does not consider the characteristics of each band in the image. Therefore, the PCA-transformed image may lose some information that reflects the spectral characteristics and accordingly distort the image spectrum. Under these circumstances, Fig. 6(b) shows more misclassification errors (i.e., red and purple pixels). Finally, Fig. 6(c) shows that the mapped landslides based on ICA-based MRF seems to coincide with the landslide boundaries. ICA can eliminate the redundant information between the original images, and effectively separate the changed information. Thus, ICA-based MRF [see Fig. 6(c)] can detect landslides (blue pixels) more completely and accurately.

In the multithreshold algorithm, T is to determine the lower threshold of each training sample for landslides and nonlandslides. The principles of change detection using CVA, PCA, and ICA are different, so we need to manually adjust T to ensure that an appropriate threshold for training sample generation. Second, ΔT is an incremental value of uncertain pixels for the further MRF analysis. Thus, pixels in these uncertain areas can be intelligently reclassified into landslides or nonlandslides through MRF. In this study, fewer parameter adjustments and less errors were introduced, which greatly improved the intelligent perception and the accuracy of landslide mapping.

Sichuan–Tibet Railway crosses the Garze Luhuo and Yarlung Zangbo seismic zones, with active geological structures. Under extreme active tectonics, the geological conditions along the railway are very complicated, and geological disasters such as landslides, debris flows, mudslides, rock falls, and mud outbursts may occur frequently. The Ya'an–Nyingchi section of the Sichuan–Tibet Railway is located on the Qinghai–Tibet Plateau and its marginal area, which was experiencing uplift by the large-scale collision and compression of the Indian Ocean and Eurasian plates. The stratum rocks along the route are complex and changeable, and the climate is severe, which produces strong internal and external dynamic geological effects, leading to frequent disasters. Therefore, mountain disasters caused by numerous factors are the key issues for the Sichuan–Tibet Railway project. This is the motivation of this study to propose a method that can automatically generate CDIs to separate the main information and noises for highlighting land cover changes. In particular, the proposed MRF algorithm can fully consider the spectral and spatial neighborhood information of the image, which can ensure an accurate landslide mapping results that can be obtained under complex geological conditions, thereby intelligently extracting landslide objects. The analysis results have shown that the ICA-based MRF can detect landslides along the railway with complex geological environment completely and accurately. This finding has important implications for disaster prevention and mitigation in the safe construction of road and railway projects. The subsequent research may aim at typical landslide disasters, combining the triggering mechanism and evolution process, for a further risk

mitigation on railway construction. Thus, studies regarding the advanced approaches to precise landslide mapping along the Sichuan–Tibet Railway would be particularly worthwhile.

Intelligent approaches such as machine learning, logistic regression, artificial neural network, and random forest have been widely applied in landslide susceptibility assessment [38]–[46]. Further study may also integrate intelligent landslide mapping with landslide susceptibility and hazard assessment for a more reliable spatial and temporal prediction of potential disasters along Sichuan–Tibet Railway. In addition, considering interferometric synthetic aperture radar has been proven particularly useful to retrieve subtle ground deformation [47], [48], it can be included for early warning of surface displacement at millimeter precision, which is difficult to be captured by optical measurements.

VI. CONCLUSION

The main goal of this study is to evaluate the applicability and effectiveness of an intelligent change detection-based MRF method for landslide migration area perception along Sichuan–Tibet Railway that is constructed in a complex geological condition. In particular, we experimented the proposed method to map the coseismic landslide migration areas that were triggered by the 2017 Nyingchi earthquake event, which has posed great threats on the railway construction. We quantitatively compared the mapping results of CVA-, PCA-, and ICA-based MRF with reference to the manually prepared ground truth map. The quantitative evaluations show that the ICA-based MRF is superior to the CVA- and PCA-based MRF for landslide perception in terms of both accuracy (86.70%), F1-score (0.81), and Kappa coefficient (0.71). The experimental results in this study justify the advantages of the proposed method using change detection-based MRF: First, it can achieve an intelligent perception of landslide migration area mapping with less parameter tuning; Second, it shows strong applicability in landslide mapping under a complicated environment with steep terrain, complex geological settings, and active tectonics along Sichuan–Tibet Railway. The developed approach has important implication for wider practices in the future. Prospective studies may derive the landslide formation and morphological characteristics from the mapped landslide migration areas, for further hazard mitigation and risk management along the railway.

REFERENCES

[1] H. J. Laimer, "Anthropogenically induced landslides—A challenge for railway infrastructure in mountainous regions," *Eng. Geol.*, vol. 222, pp. 92–101, May 2017.

[2] Y. Zhang, Z. Yang, C. Guo, T. Wang, D. H. Wang, and G. Du, "Predicting landslide scenes under potential earthquake scenarios in the Xianshuihe fault zone, Southwest China," *J. Mountain Sci.*, vol. 14, pp. 1262–1278, Jul. 2017.

[3] W. Wang, J. Li, and Z. Han, "Comprehensive assessment of geological hazard safety along railway engineering using a novel method: A case study of the Sichuan–Tibet Railway, China," *Geomatics, Natural Hazards Risk*, vol. 11, pp. 1–21, Dec. 2019.

[4] R. Wu, Y. Zhang, C. Guo, Z. Yang, J. Tang, and F. Su, "Landslide susceptibility assessment in mountainous area: A case study of Sichuan–Tibet Railway, China," *Environ. Earth Sci.*, vol. 79, pp. 1–16, Mar. 2020.

[5] M. Sahana and H. Sajjad, "Evaluating effectiveness of frequency ratio, fuzzy logic and logistic regression models in assessing landslide susceptibility: A case from Rudraprayag district, India," *J. Mountain Sci.*, vol. 14, pp. 2150–2167, Jun. 2017.

[6] A. Kumar, R. K. Sharma, and V. K. Bansal, "GIS-based comparative study of information value and frequency ratio method for landslide hazard zonation in a part of mid-Himalaya in Himachal Pradesh," *Innovative Infrastruct. Solution*, vol. 4, pp. 274–287, Jun. 2019.

[7] F. G. Murillo-García, I. Alcantara-Ayala, F. Ardizzone, M. Cardinali, F. Fiourucci, and F. Guzzetti, "Satellite stereoscopic pair images of very high resolution: A step forward for the development of landslide inventories," *Landslides*, vol. 12, pp. 277–291, 2015.

[8] F. Guzzetti, A. C. Mondini, M. Cardinali, F. Fiorucci, M. Santangelo, and K.-T. Chang, "Landslide inventory maps: New tools for an old problem," *Earth-Sci. Rev.*, vol. 112, pp. 42–66, Apr. 2012.

[9] S. Ghosh et al., "Generating event-based landslide maps in a data-scarce Himalayan environment for estimating temporal and magnitude probabilities," *Eng. Geol.*, vol. 128, pp. 49–62, 2012.

[10] Z. Li, W. Shi, S. W. Myint, P. Lu, and Q. Wang, "Semi-automated landslide inventory mapping from bitemporal aerial photographs using change detection and level set method," *Remote Sens. Environ.*, vol. 175, pp. 215–230, Mar. 2016.

[11] R. N. Keyport, T. Oommen, T. R. Martha, K. S. Sajinkumar, and J. S. Gierke, "A comparative analysis of pixel- and object-based detection of landslides from very high-resolution images," *Int. J. Appl. Earth Observ. Geoinf.*, vol. 64, pp. 1–11, Feb. 2018.

[12] L. Drăguţ, D. Tiede, and S. R. Levick, "ESP: A tool to estimate scale parameter for multiresolution image segmentation of remotely sensed data," *Int. J. Geographical Inf. Sci.*, vol. 24, pp. 859–871, Mar. 2010.

[13] P. Lu, A. Stumpf, N. Kerle, and N. Casagli, "Object-oriented change detection for landslide rapid mapping," *IEEE Geosci. Remote Sens. Lett.*, vol. 8, no. 4, pp. 701–705, Jul. 2011.

[14] T. R. Martha, N. Kerle, V. Jetten, C. J. van Westen, and K. V. Kumar, "Object-oriented analysis of multi-temporal panchromatic images for creation of historical landslide inventories," *ISPRS J. Photogrammetry Remote Sens.*, vol. 67, pp. 105–119. Jan. 2012.

[15] T. R. Martha, N. Kerle, C. J. van Westen, V. Jetten, and K. V. Kumar, "Segment optimization and data-driven thresholding for knowledge-based landslide detection by object-based image analysis," *IEEE Trans. Geosci. Remote Sens.*, vol. 49, no. 12, pp. 4928–4943, Dec. 2011.

[16] T. Chen, J. Trinder, and R. Niu, "Object-oriented landslide mapping using ZY-3 satellite imagery, random forest and mathematical morphology, for the Three-Gorges Reservoir, China," *Remote Sens.*, vol. 9, no. 4, Mar. 2017.

[17] A. C. Mondini, F. Guzzetti, P. Reichenbach, M. Rossi, M. Cardinali, and F. Ardizzone, "Semi-automatic recognition and mapping of rainfall induced shallow landslides using optical satellite images," *Remote Sens. Environ.*, vol. 115, pp. 1743–1757, Jul. 2011.

[18] Z. Lv, T. Liu, P. Zhang, J. A. Benediktsson, and Y. Chen, "Land cover change detection based on adaptive contextual information using bitemporal remote sensing images," *Remote Sens.*, vol. 10, Jun. 2018.

[19] C. Kurtz, A. Stumpf, J. P. Malet, P. Gancarski, A. Puissant, and N. Passat, "Hierarchical extraction of landslides from multiresolution remotely sensed optical images," *ISPRS J. Photogrammetry Remote Sens.*, vol. 87, pp. 122–136, Jan. 2014.

[20] Y. Yi and W. Zhang, "A new deep-learning-based approach for earthquake-triggered landslide detection from single-temporal RapidEye satellite imagery," *IEEE J. Sel. Topics Appl. Earth Observ. Remote Sens.*, vol. 13, pp. 6166–6176, Oct. 2020.

[21] C. Ye et al., "Landslide detection of hyperspectral remote sensing data based on deep learning with constrains," *IEEE J. Sel. Topics Appl. Earth Observ. Remote Sens.*, vol. 12, no. 12, pp. 5047–5060, Dec. 2019.

[22] H. Cai, T. Chen, R. Niu, and A. Plaza, "Landslide detection using densely connected convolutional networks and environmental conditions," *IEEE J. Sel. Topics Appl. Earth Observ. Remote Sens.*, vol. 14, pp. 5235–5247, May 2021.

[23] D. Duric, A. Mladenovic, M. Pesic-Georgiadis, M. Marjanovic, and B. Abolmasov, "Using multiresolution and multitemporal satellite data for post-disaster landslide inventory in the Republic of Serbia," *Landslides*, vol. 14, pp. 1467–1482, Jun. 2017.

[24] P. Lu, Y. Qin, Z. Li, A. C. Mondini, and N. Casagli, "Landslide mapping from multi-sensor data through improved change detection-based Markov random field," *Remote Sens. Environ.*, vol. 231, Sep. 2019a, Art. no. 111235.

[25] K. Hu, X. Zhang, Y. You, X. Hu, W. Liu, and Y. Li, "Landslides and dammed lakes triggered by the 2017 Ms6.9 Milin earthquake in the Tsangpo Gorge," *Landslides*, vol. 16, pp. 993–1001, Mar. 2019.

[26] K. Li, X. Xu, E. Kirby, F. Tang, and W. Kang, "Late Quaternary paleoseismology of the Milin fault: Implications for active tectonics along the Yarlung Zangbo Suture, Southeastern Tibet Plateau," *Tectonophysics*, vol. 731, pp. 64–72. Apr. 2018.

[27] P. Lu, W. Shi, Q. Wang, Z. Li, Y. Qin, and X. Fan, "Co-seismic landslide mapping using Sentinel-2 10-m fused NIR narrow, red-edge, and SWIR bands," *Landslides*, vol. 18, pp. 2017–2037, Feb. 2021.

[28] P. Tapponnier *et al.*, "Oblique stepwise rise and growth of the Tibet Plateau," *Science*, vol. 294, pp. 1671–1677, Nov. 2001.

[29] M. Drusch *et al.*, "Sentinel-2: ESA's optical high-resolution mission for GMES operational services," *Remote Sens. Environ.*, vol. 120, pp. 25–36, May 2012.

[30] M. Pesaresi, C. Corbane, A. Julea, A. Florczyk, V. Syrris, and P. Soille, "Assessment of the added-value of Sentinel-2 for detecting built-up areas," *Remote Sens.*, vol. 8, May 2016.

[31] M. Immitzer, F. Vuolo, and C. Atzberger, "First experience with Sentinel-2 data for crop and tree species classifications in central Europe," *Remote Sens.*, vol. 8, Feb. 2016.

[32] D. P. Roy, J. Li, H. K. Zhang, L. Yan, H. Huang, and Z. Li, "Examination of Sentinel-2A multi-spectral instrument (MSI) reflectance anisotropy and the suitability of a general method to normalize MSI reflectance to nadir BRDF adjusted reflectance," *Remote Sens. Environ.*, vol. 199, no. 15, pp. 25–38, Sep. 2017.

[33] V. S. Martins, C. C. F. Barbosa, L. A. S. De Carvalho, D. S. F. Jorge, F. D. L. Lob, and E. M. L. D. M. Novo, "Assessment of atmospheric correction methods for Sentinel-2 MSI images applied to amazon floodplain lakes," *Remote Sens.*, vol. 9, Apr. 2017.

[34] S. Sartajvir, S. Vishakha Soo, T. Ajay Kumar, P. Shivendur, and K. Ravneet Kaur, "Qualitative and quantitative analysis of topographically derived CVA algorithms using MODIS and landsat-8 data over western Himalayas, India," *Quaternary Int.*, vol. 575-576, pp. 85–95, Feb. 2021.

[35] Z. Li, W. Shi, P. Lu, L. Yan, Q. Wang, and Z. Miao, "Landslide mapping from aerial photographs using change detection-based Markov random field," *Remote Sens. Environ.*, vol. 187, pp. 76–90, Dec. 2016.

[36] F. Huang *et al.*, "Regional terrain complexity assessment based on principal component analysis and geographic information system: A case of Jiangxi Province, China," *ISPRS Int. J. Geo-Inf.*, vol. 9, Sep. 2020.

[37] R. Comert, "Investigation of the effect of the dataset size and type in the earthquake-triggered landslides mapping: A case study for the 2018 Hokkaido Iburu landslides," *Frontiers Earth Sci.*, vol. 9, Feb. 2021, Art. no. 633665.

[38] T. Chen, R. Niu, B. Du, and Y. Wang, "Landslide spatial susceptibility mapping by using GIS and remote sensing techniques: A case study in Zigui county, the Three Georges Reservoir, China," *Environ. Earth Sci.*, vol. 73, no. 9, pp. 5571–5583, May 2015.

[39] T. Chen, R. Niu, and X. Jia, "A comparison of information value and logistic regression models in landslide susceptibility mapping by using GIS," *Environ. Earth Sci.*, vol. 75, no. 10, pp. 1–16, May 2016.

[40] T. Chen *et al.*, "Mapping landslide susceptibility at the Three Gorges Reservoir, China, using gradient boosting decision tree, random forest and information value models," *J. Mountain Sci.*, vol. 17, no. 3, pp. 670–685, Mar. 2020.

[41] P. Lu, F. Catani, V. Tofani, and N. Casagli, "Quantitative hazard and risk assessment for slow-moving landslides from persistent scatterer interferometry," *Landslides*, vol. 11, no. 4, pp. 685–696, Aug. 2014.

[42] Y. Song *et al.*, "Landslide susceptibility mapping based on weighted gradient boosting decision tree in Wanzhou section of the Three Gorges Reservoir area (China)," *ISPRS Int. J. Geo-Inf.*, vol. 8, no. 1, p. 8, 2019.

[43] J. Song, Y. Wang, Z. Fang, L. Peng, and H. Hong, "Potential of ensemble learning to improve tree-based classifiers for landslide susceptibility mapping," *IEEE J. Sel. Topics Appl. Earth Observ. Remote Sens.*, vol. 13, pp. 4642–4662, Aug. 2020.

[44] Y. Chen, D. Ming, X. Ling, X. Lv, and C. Zhou, "Landslide susceptibility mapping using feature fusion-based CPCNN-ML in Lantau Island, Hong Kong," *IEEE J. Sel. Topics Appl. Earth Observ. Remote Sens.*, vol. 14, pp. 3625–3639, Mar. 2021.

[45] Q. Zhu, L. Chen, H. Hu, S. Pirasteh, H. Li, and X. Xie, "Unsupervised feature learning to improve transferability of landslide susceptibility representations," *IEEE J. Sel. Topics Appl. Earth Observ. Remote Sens.*, vol. 13, pp. 3917–3930, Jul. 2020.

[46] C. Zhou, K. Yin, Y. Cao, E. Intrieri, B. Ahmed, and F. Catani, "Displacement prediction of step-like landslide by applying a novel Kernel extreme learning machine method," *Landslides*, vol. 15, no. 5, pp. 2211–2225, 2018.

[47] P. Lu, S. Bai, V. Tofani, and N. Casagli, "Landslides detection through optimized hot spot analysis on persistent scatterers and distributed scatterers," *ISPRS J. Photogrammetry Remote Sens.*, vol. 156, pp. 147–159, Oct. 2019b.

[48] P. Lu *et al.*, "Lake outburst accelerated permafrost degradation on Qinghai-Tibet Plateau," *Remote Sens. Environ.*, vol. 249, Nov. 2020, Art. no. 112011.

Wenyang Shi received the B.S. degree in surveying and mapping engineering from Shandong University of Science and Technology, Qingdao, China, in 2019. She is currently working toward the master's degree in photogrammetry and remote sensing with the College of Surveying and Geo-Informatics, Tongji University, Shanghai, China.

Her research interests include remote sensing image data processing, and intelligent information extraction for natural hazard applications.

Ping Lu received the M.S. degree in earth observations from Katholieke Universiteit Leuven, Leuven, Belgium, in 2007, and the Ph.D. degree in earth sciences from the University of Firenze, Firenze, Italy, in 2011.

He is currently an Associate Professor with the College of Surveying and Geo-Informatics, Tongji University, Shanghai, China. His research interests include artificial intelligence techniques applied to geosciences and remote sensing.